

UC Berkeley

UC Berkeley Previously Published Works

Title

The Drosophila Pioneer Factor Zelda Modulates the Nuclear Microenvironment of a Dorsal Target Enhancer to Potentiate Transcriptional Output.

Permalink

<https://escholarship.org/uc/item/68042642>

Journal

Current Biology, 29(8)

Authors

Yamada, Shigehiro
Whitney, Peter
Huang, Shao-Kuei
et al.

Publication Date

2019-04-22

DOI

10.1016/j.cub.2019.03.019

Peer reviewed



Published in final edited form as:

Curr Biol. 2019 April 22; 29(8): 1387–1393.e5. doi:10.1016/j.cub.2019.03.019.

The *Drosophila* pioneer factor Zelda modulates the nuclear microenvironment of a Dorsal target enhancer to potentiate transcriptional output

Shigehiro Yamada^{1,6}, Peter H. Whitney^{1,6}, Shao-Kuei Huang¹, Elizabeth C. Eck², Hernan G. Garcia^{2,3,4,5}, Christine A. Rushlow^{1,7,*}

¹Department of Biology, New York University, New York, NY 10003 U.S.A.

²Biophysics Graduate Group, University of California at Berkeley, Berkeley, CA 94720 U.S.A

³Department of Molecular and Cellular Biology, University of California at Berkeley, Berkeley, CA 94720 U.S.A

⁴Department of Physics, University of California at Berkeley, Berkeley, CA 94720 U.S.A

⁵Quantitative Biosciences-QB3, University of California at Berkeley, Berkeley, California 94720 U.S.A

⁶These author contributed equally

⁷Lead contact

Summary

Connecting the developmental patterning of tissues to the mechanistic control of RNA polymerase II remains a long term goal of developmental biology. Many key elements have been identified in the establishment of spatial-temporal control of transcription in the early *Drosophila* embryo, a model system for transcriptional regulation. The dorsal/ventral axis of the *Drosophila* embryo is determined by the graded distribution of Dorsal (Dl), a homologue of the NF- κ B family of transcriptional activators found in humans [1,2]. A second maternally deposited factor, Zelda (Zld), is uniformly distributed in the embryo and is thought to act as a pioneer factor, increasing enhancer accessibility for transcription factors such as Dl [3–9]. Here we utilized the MS2 live imaging system to evaluate the expression of the Dl target gene *short gastrulation (sog)* to better

*Correspondence: chris.rushlow@nyu.edu.

Author Contributions

CAR, HGG, and PHW designed the overall study. ECE designed and prepared the MS2v5(-TAG) loops vector. SY made the *sog* enhancer-MS2v5(-TAG) reporter constructs and carried out the live imaging experiments. CAR, PHW and SH carried out the assays in fixed embryos. PHW conceived the ideas and wrote code for the computational image analysis. PHW wrote the draft manuscript and all authors contributed to revisions.

Publisher's Disclaimer: This is a PDF file of an unedited manuscript that has been accepted for publication. As a service to our customers we are providing this early version of the manuscript. The manuscript will undergo copyediting, typesetting, and review of the resulting proof before it is published in its final citable form. Please note that during the production process errors may be discovered which could affect the content, and all legal disclaimers that apply to the journal pertain.

Declaration of Interests

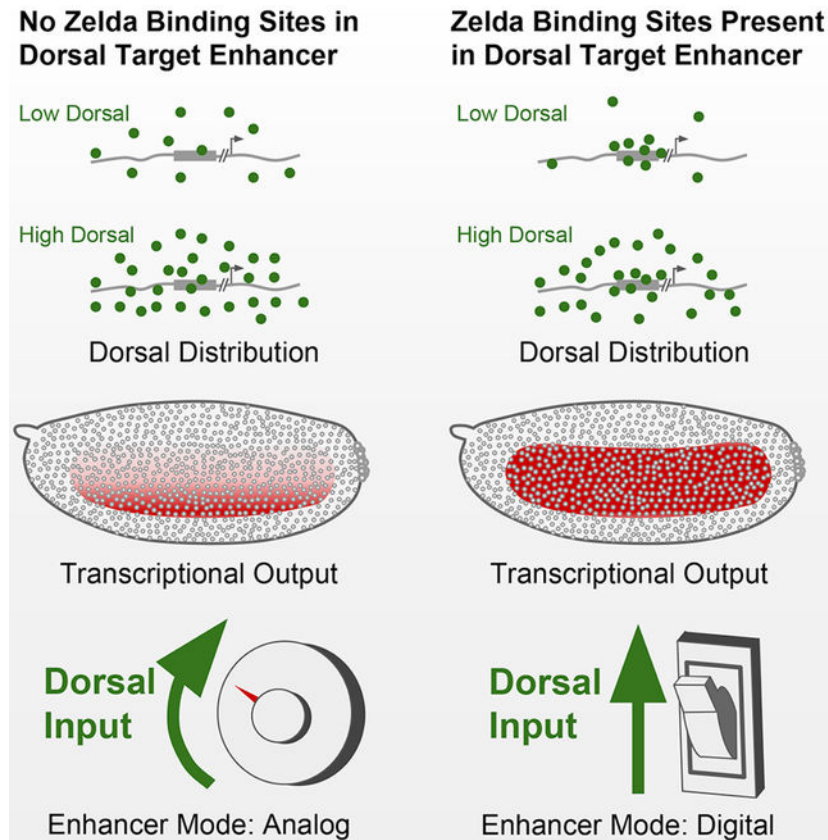
The authors declare no competing interests.

Supplemental Information

Supplemental items include one figure (Figure S1 in Supplemental PDF) and six videos (Videos S1–S6).

understand how a pioneer factor affects the kinetic parameters of transcription. Our experiments indicate that Zld modifies probability of activation, the timing of this activation, and the rate at which transcription occurs. Our results further show that this effective rate increase is due to an increased accumulation of DI at the site of transcription, suggesting that transcription factor “hubs” induced by Zld [10] functionally regulate transcription.

Graphical Abstract



eTOC Blur

Drosophila embryos establish a graded distribution of Dorsal protein to define the dorsal/ventral axis in early development. Yamada, Whitney et al. demonstrate how Zelda allows a cis-regulatory element to unify gene expression over a broad dynamic range of the Dorsal gradient by raising the local concentration of Dorsal at the enhancer.

Results

Our study focused on the DI target gene *sog* as its expression domain spans a large dynamic range of the DI gradient, allowing us to examine how Zld potentiates DI activity across the dorsal/ventral axis. Previous experiments have demonstrated that the lateral stripe of *sog* expression narrows dramatically in *zld* null embryos [5,11] (Figures 1A and 1B), and that progressively removing Zld DNA binding sites from the *sog* shadow (distal) enhancer shrinks the domain of activation of reporter genes in a linear manner [7]. In order to

understand how Zld influences transcription at different points along the Dl gradient, we revisited these constructs with the aim of visualizing transcription in real time by adding 24 MS2 loops to the 5' end of the *lacZ* reporter. Since previously utilized MS2 loops [12–15] contained potential Zld binding sites [16], we revised the MS2v5 [17] sequence to make a Zld binding site-free non-repetitive version, referred to as MS2v5(-TAG) (see STAR Methods). Constructs also contained either the *sog* shadow (distal) enhancer [18,19] with its three native canonical Zld binding sites, CAGGTAG (hereafter referred to as “3TAG”), or without these sites (hereafter referred to as “0TAG”) (Figure 1C; see STAR Methods for enhancer sequences; [7]). The narrowing effect of removing Zld binding sites was confirmed by *in situ* hybridization (Figures 1D and 1E).

By crossing these transgenic reporter lines to females expressing the MCP (MS2 Coat Protein)-GFP fusion gene during oogenesis [14], we visualized the transcriptional activation of each reporter as fluorescent foci (see Figure 1C and STAR Methods). These embryos also express H2Av(histone 2A variant)-RFP [20], allowing us to track nuclear cycles and record transcriptional activation events in space and time. We performed confocal live imaging over the course of nuclear cycles 10 to 14 (NC10-NC14), tracking the activation of the 3TAG and 0TAG reporter genes (Videos S1–S2). To validate that the MS2 transgenes behaved as expected, we examined transcriptional activation events in space and time and compared those to expression as assessed by conventional *in situ* analysis. We find that the 3TAG construct is activated as early as NC10, while activation of the 0TAG construct is delayed until NC11–12 (Figures 2A and 2B and Videos S1–S2; also see additional Videos S3–S6), in agreement with previously published results of *sog* activation in *zld* mutants [5].

To compare the spatial differences in activation, we divided the expression domain of *sog* into five discrete zones with Zone 1 comprising the mesoderm, and all subsequent zones defined by 20 μ m width bands moving sequentially towards the dorsal midline of the embryo, diagrammed in Figure 2C. The *in situ* experiments predict that the most dorsal zones imaged would show few active nuclei in 0TAG embryos, and this was the case. While 3TAG embryos showed similar numbers of active nuclei in each zone across all cycles (NC12-NC14), with the exception of Zone 1 in NC14 due to ventral repression by Snail (Figure 2D), in 0TAG embryos, the more dorsal the zone, the fewer the number of active nuclei (Figure 2E). Collectively, these qualitative observations are in accordance with what is currently known about how Zld participates in transcriptional activation, and provide evidence that our transgenes are faithfully reporting on the transcriptional activity of *sog* in the presence or absence of Zld.

In addition to allowing qualitative assessment of transcriptional activation, MS2 reporters continually output information on the state of transcription over time, enabling an analysis of the timing of each activation event within a nuclear cycle [14]. This was performed by measuring the time between anaphase of NC12 and the appearance of fluorescent foci in NC13, and plotting the results as cumulative distribution curves (Figures 2F–2H). This analysis showed that nuclei in 3TAG embryos express simultaneously across the domain of expression (Figure 2G; Video S1). In stark contrast, we observed a significant position-dependent delay of activation in 0TAG embryos where the ventral nuclei activate transcription well before lateral nuclei (Figure 2H; Video S2). This is presumably due to the

highly dynamic nature of the DI gradient, whereby DI levels increase within and across nuclear cycles [21–23]. Here, the 0TAG reporter is effectively acting as a readout for nuclear DI concentration, suggesting that in the absence of Zld binding sites the *sog* enhancer responds to DI levels in a concentration-dependent manner, rather than the binary switch-like response seen in the presence of Zld.

Knowing that activation is altered in 0TAG embryos, we next examined the internal kinetic features of transcription. We focused principally on two phases of transcription, which are described in Figures 3A and 3B using representative nuclei from each genotype at NC13, with the signal over time quantified in Figures 3C and 3D. The first was “ramp-up”, an early phase where polymerase molecules first begin to elongate as transcription begins. Here the rise in MS2 signal is attributed to polymerases accumulating over the gene body as they transcribe the MS2 loops and continue to elongate. The length of the ramp-up phase is commonly thought of as the time in which a single polymerase molecule has traversed the entire gene body [14]. The transition to the next phase, “steady-state” transcription, is reached when the rate of polymerase loading is matched by rate of polymerase unloading, diagrammed in Figure 3E. Here the MS2 signal levels off and fluctuates within a narrow range as there is no net gain of nascent transcripts. We have included an equation demonstrating that the signal strength at steady-state transcription can be understood as the average gap between polymerase molecules on the gene body (Figure 3E).

Using the duration of the ramp-up phase, which can be referred to as the “time to steady state”, we can calculate the number of nuclei that have reached steady-state transcription as cumulative distribution curves, with the percentage of all active nuclei at steady-state plotted over time (Figure 3F and 3G). There is a striking similarity between the two genotypes, indicating that Zld does not act on the speed of polymerase. In addition, the time to steady-state is similar in each of the different zones, suggesting that nuclear DI concentration has little influence on polymerase elongation rate. In contrast, when signal intensity values of steady-state transcription are averaged for each nucleus (Figure 3H) it appears that both Zld and DI are modulating the strength of transcription. Similar to our observations regarding the onset of transcriptional activation, the 3TAG reporter shows comparable max output across multiple zones until the most extreme end of the DI gradient (Zone 5), whereas the 0TAG reporter shows a progressive loss of max output across the entire gradient (Figure 3F), indicating that transcriptional output rate has become a function of nuclear DI concentration. These results suggest Zld acts upstream of elongation, for example, to either increase RNA polymerase II loading or decrease the length of pausing experienced by a given polymerase molecule. Either of these regulatory steps would affect the mean spacing of polymerase molecules at max output.

This behavior of Zld inducing uniform transcriptional activation and output across a transcriptional activator gradient could be explained by Zld’s reported ability to promote the formation of transcription factor “hubs” [10,24,25]. By raising the local concentration of DI at the site of transcription, Zld may effectively flatten the gradient of DI experienced by the enhancer, and therefore unify the levels of transcriptional output in regions of low level DI. To test this hypothesis, we used a previously described method to examine transcription factor enrichment at sites of nascent transcript formation in *Drosophila* embryos [26,27]. By

costaining fixed embryos with an anti-DI antibody and a single molecule (sm) FISH probe targeting the *lacZ* reporter transcript [28], we could quantify the concentration of DI protein adjacent to foci of transcription. Figure 4A shows the DI gradient at comparable positions in 3TAG and 0TAG embryos. Signal overlap between puncta of DI staining and *lacZ* staining, the presumed site of transcription, can be seen in 3D contour maps where the surface represents the level of DI antibody signal and the site of transcription is mapped onto the texture of the contour. We classified nuclei as either having a High, Mid, or Low level of DI based on binning all nuclei imaged according to their average DI signal intensity, which correspond spatially to Zones 1, 2, and 3 in Figures 2 and 3.

Figure 4C uses a modified approach demonstrated by Tsai et al. [29], where the radial intensity of the DI antibody stain is plotted to visualize the nuclear microenvironment that surrounds a site of active transcription (*lacZ* staining). Because the nuclear concentration of DI changes across the gradient, we divided voxel intensity by the average voxel intensity found within a nucleus. In this way, we could normalize across nuclei by defining our measurement as a unitless index describing the relative enrichment of signal at a given site of transcription, where a value of 1 indicates no enrichment. Additionally, we included a set of random points within nuclei as a control. For a full breakdown of individual enrichment curves, see Figure S1. As predicted, we see a progressive loss in enrichment over the gradient in 0TAG embryos, and a measurable gain in enrichment in 3TAG embryos, indicating that Zld's ability to drive higher transcriptional output is based on enhancing the local concentration of existing transcriptional activators rather than utilizing an additional Zld specific activation pathway. Importantly, these results strongly suggest a functional link between Zld's reported ability to induce transcription factor aggregates [10] and transcriptional output, an important first step towards a complete understanding of Zld's ability to control gene expression.

Discussion

The precise logic governing cis-regulatory elements is still an evolving field after decades of research. The role of pioneer factors such as Zld in modifying chromatin has increased our understanding of how patterning transcription factors such as DI and Bicoid (Bcd) access their target enhancers [4,7,8,30,31], however questions persist as to the events that occur at the site of transcription. Several recent reports have suggested that the accumulation and stable association of transcription factor aggregates, or hubs, is important for proper transcriptional output [10,24,25,29]. Additionally, the *Drosophila* transcription factor Bcd is enriched in Zld hubs, particularly in nuclei with lower overall Bcd, suggesting that Zld interacts with transcription factors to raise their local concentration [24]. Our results manipulating Zld binding at the enhancer/site of transcription agree nicely with these recent findings, and for the first time suggest a direct impact of these transcription factor hubs on transcription itself.

Our experiments identify two key parameters where Zld modifies the activity of a DI-responsive enhancer. The first parameter is the onset of transcription across the domain of *sog*, where a position-dependent delay in transcriptional activation of the reporter was observed in the 0TAG embryos. We believe that the uniformity of this response is the result

of Zld's pioneering activity to ubiquitously lower the nucleosome barrier from regions of DNA in close proximity to its DNA binding motif. Freeing up enhancers may then allow DI to be bound more quickly at low concentrations, which may in turn lead to local enrichment of DI (Figure 4C). In the absence of Zld, DI must compete directly with nucleosomes to access its DNA binding sites. This competition could be more effective at high concentrations of DI, thus leading to the concentration-dependent effects observed in 0TAG. The second parameter controlled by Zld is the uniformity of the transcriptional output over the course of a nuclear cycle. Our MS2 data of 3TAG embryos showed remarkably similar levels of total transcription in all measured positions save for the most extreme dorsally-located nuclei. Our results of higher DI enrichment in 3TAG embryos in nuclei with low DI tracks well with the measurements of transcription. However, It remains to be seen if these two transcriptional parameters (timing and output) are connected by a single mechanistic step mediated by Zld binding to an enhancer.

More broadly, these experiments demonstrate the influence that Zld has on global dynamics of tissue patterning. Morphogen gradients supply positional information through an analog signal: a contiguous modulation in morphogen concentration directly encodes location along a developmental axis. When creating a broad domain of expression from this signal, a conversion from analog to digital information must occur; a varying amount of transcriptional activator, in this case DI, must be reliably converted into a uniform transcriptional response. Our work suggests that DI's interaction with Zld allows it to produce near identical transcriptional output over a large range of nuclear DI concentrations and in the absence of that interaction, output is purely reflective of the underlying gradient. As uniform transcriptional domains that span large sections of morphogen gradients are a common motif across developmental systems, we believe our work helps shed light on a common principle of cellular fate decisions.

STAR METHODS:

CONTACT FOR REAGENT AND RESOURCE SHARING

Requests for any information and requests for resources or reagents should be directed to the Lead Contact, Christine Rushlow (car2@nyu.edu)

EXPERIMENTAL MODEL AND SUBJECT DETAILS

All flies were grown on standard fly (*Drosophila melanogaster*) cornmeal-molasses-yeast media. *y[1]w[1118]*(used as wild type flies), *zld* shmir (*zld⁺*) (see "Depletion of maternal *zld*" section below) [8], and transgenic embryos (3TAG and 0TAG) were collected on yeasted grape juice agar plates. Flies of the genotype *y[1] w^{*}; P{His2Av-mRFP1}II.2; P{nos-MCPEGFP}2* (Bloomington Stock Number 60340) carried two transgenes, one on chromosome 3, *P{nos-MCPEGFP}2*, which expresses the MS2 coat protein (MCP) fused to EGFP under the control of the *nanos* promoter active in oogenesis, and the other on chromosome 2, *P{His2Av-mRFP1}II.2*, which expresses RFP-tagged His2Av in all cells under the control of *His2Av*. MS2 transgenes were constructed in the following manner: MS2 loop sequences were revised since previously used MS2 loops [12–14,16,17] contained potential Zld binding sites [5,14,16]. The new MS2 loops sequence, MS2v5(-TAG) (see

Method Details for DNA sequence) was placed in between the *eve* minimal promoter and a *lacZ* reporter gene (pib-evepr-ms2v5(-TAG)-*lacZ* plasmid), then subcloned into an attB vector (pBPhi) containing *sog* enhancers with (3TAG) or without (0TAG) Zld binding sites [7] (Method Details). Transgenic lines carrying these constructs were generated by phiC31 integration in the 53B2 landing site (VK00018), Bloomington stock number 9736 [32,33] by BestGene.

METHOD DETAILS

Depletion of maternal *zld*—Embryos were collected from females depleted of *zld* RNAs by RNAi prepared in two crosses [8]: 1st cross ♀ +; +; UAS-shRNA-*zld* X ♂ P{*COG*-GAL4:VP16}; P{Gal4-*nos*.NGT}40; P{*nos*-Gal4-VP16}; 2nd cross G1♀ P{*COG*-GAL4:VP16}/+; P{Gal4-*nos*.NGT}40/+; P{*nos*-Gal4-VP16}/UAS-shRNA-*zld* X ♂ *yw*

Sequence of the *sog* 3TAG and 0TAG enhancers—*sog* 3TAG

426 bp enhancer sequence (Zld binding site in red):

```
GTTTCAGCGGAACAGGTAGGCTGGTTCGATCGGAAATCCCACCATACACATGTGG
CTATAATGCCAACGGCATCGAGGTGCGAAAACAGATGCAGCCTCATAAAAGGGGC
GCAGATAAGGTTCGCGGTTGCGTGGGAAAAGCCCATCCGACCAGGACCAGGACGA
AGCAGTGCGGTTGGCGCATCATTGCCGCCATATCTGCTATTCTACCTGCGTGGCC
ATGGCGATATCCTTGTGCAAGGATAAGGAGCGGGGATCATAAAACGCTGTGCGTT
TTGTTTATGCTGCTTATTTAAATTGGCTTCTTGGCGGGCGTTGCAACCTGGTGCTA
GTCCCAATCCCAATCCCAATTCCAATCCCAATCCATATAACCATATCCAATGCATTCT
ACCTGTCCTGGGAATTTCCGATCTGGCCGCACCCATAT
```

sog 0TAG

426 bp enhancer sequence (mutated Zld binding site in red):

```
GTTTCAGCGGAACCAACAAGCTGGTTCGATCGGAAATCCCACCATACACATGTGG
CTATAATGCCAACGGCATCGAGGTGCGAAAACAGATGCAGCCTCATAAAAGGGGC
GCAGATAAGGTTCGCGGTTGCGTGGGAAAAGCCCATCCGACCAGGACCAGGACGA
AGCAGTGCGGTTGGCGCATCATTGCCGCCATATCTGCTATTCTTGTGGCGTGGCC
ATGGCGATATCCTTGTGCAAGGATAAGGAGCGGGGATCATAAAACGCTGTGCGTT
TTGTTTATGCTGCTTATTTAAATTGGCTTCTTGGCGGGCGTTGCAACCTGGTGCTA
GTCCCAATCCCAATCCCAATTCCAATCCCAATCCATATAACCATATCCAATGCATTTT
GTTGGTCTGGGAATTTCCGATCTGGCCGCACCCATAT
```

***in situ* hybridization**—Embryos were collected and aged to be 1–3 hours old at room temperature and dechorionated in Clorox for two minutes. They were then fixed in 4% formaldehyde (1X PBS) and an equal volume of heptane for 25 minutes while shaking vigorously. Devitellinization was performed by pipetting off the bottom fixative phase and adding 4 ml of methanol and shaking vigorously for 30 seconds. Embryos were rinsed in methanol and transferred to ethanol for storage at –20 degrees C. Hybridization of fixed embryos used a standard *in situ* hybridization (ISH) protocol and DIG-labeled *sog* cDNA or

eaaaccagtcgaaggtcaaacctctccacaaaactgcgaagcaggatcaccgcttcgccattccaacatacacaatacaaaaaca
 attagtcgtacagcatcagcgtacgaccacgcatcagtgactactatcaaaaacaaaccgttcagcaacagcgaacggtacacacg
 gaaaaatcaactggtttacaatacgaagacgagcagcgtttcaactattacgaaaacatccgagggcgtacgcaacagcgtacg
 cccggcggaaacctcacaacacgacaacggaagcacgaacacggcttcgccgacaaccacaacttacaacgacgc
 aaacggtgcaggatcaccgcaccgtacatcaaacctcagatctcatt

MS2v5 sequence (24 old loops highlighted in grey; Zld sites in purple)—

ggatcctacggtacttattgccaagaaagcacgagcatcagccgtgcctccagggtcgaatcttcaaacgacgacgatcagcgtcgc
 tccagtattccagggttcacgatcctacggtacttattgccaagaaagcacgagcatcagccgtgcctccagggtcgaatcttcaaac
 gacgacgatcagcgtcgtccagtattccagggttcacgatcctacggtacttattgccaagaaagcacgagcatcagccgtgc
 ctccagggtcgaatcttcaaacgacgacgatcagcgtcgtcctccagtattccagggttcacgatcctacggtacttattgccaagaa
 gcacgagcatcagccgtgcctccagggtcgaatcttcaaacgacgacgatcagcgtcgtcctccagtattccagggttcacgatccta
 cgggtacttattgccaagaaagcacgagcatcagccgtgcctccagggtcgaatcttcaaacgacgacgatcagcgtcgtcctccagtatt
 ccagggttcacgatcctacggtacttattgccaagaaagcacgagcatcagccgtgcctccagggtcgaatcttcaaacgacgacg
 atcagcgtcgtcctccagtattccagggttcacgatcctacggtacttattgccaagaaagcacgagcatcagccgtgcctccagggt
 cgaatcttcaaacgacgacgatcagcgtcgtcctccagtattccagggttcacgatcctacggtacttattgccaagaaagcacgag
 catcagccgtgcctccagggtcgaatcttcaaacgacgacgatcagcgtcgtcctccagtattccagggttcacgatcctacggtactt
 attgccaagaaagcacgagcatcagccgtgcctccagggtcgaatcttcaaacgacgacgatcagcgtcgtcctccagtattccagggt
 tcatcagatcctacggtacttattgccaagaaagcacgagcatcagccgtgcctccagggtcgaatcttcaaacgacgacgatcagc
 gtcgtcctccagtattccagggttcacgatcctacggtacttattgccaagaaagcacgagcatcagccgtgcctccagggtcgaatctt
 caaacgacgacgatcagcgtcgtcctccagtattccagggttcacgatcctacggtacttattgccaagaaagcacgagcatcagc
 cgtgcctccagggtcgaatcttcaaacgacgacgatcagcgtcgtcctccagtattccagggttcacgatcctacggtacttattgccaagaaagcacgagcatcagc
 sequence

Live imaging—Virgin females maternally expressing MCP-GFP and H2Av-RFP were crossed with males of the MS2 reporter lines. 0–1 hour embryos were collected, dechorionated, and transferred onto a breathable membrane (Lumox Film, Sarstedt AG & Co.; Nümbrecht, Germany) in the middle of a plastic microscope slide (3D printed by Sculpteo; Créteil, France). Live imaging was performed using a Leica SP8 63X objective lens with the following settings: optical sections: 512×512 pixels, 30 z stacks 0.69 μm apart, 12bit; zoom: 1.7; time resolution: 40 seconds per frame. Laser power was measured using the X-Cite power meter, model No.XR2100) and set at 70% (main), 30% (488nm), and 10% (554nm). Embryos were imaged for approximately two hours, typically from nc 10 to early nc 14, as *sog* refines rapidly during mid-late nc 14 due to dynamic regulation by other factors [35].

High Resolution Imaging—Antibody and smFISH stained embryos with either 3TAG or OTAG MS2 reporters were imaged using a LSM Zeiss 880 confocal microscope with 100X objective using the following settings: 1132×1132 pixels with 0.14 μm z-stack step size, 16bit, 1.8 zoom. Laser power was set at 1% (405nm), 5% (488nm), 15% (633nm). All images were captured using the the Airyscan detector array. Post-processing was carried out using the ZEN2012 software “Airyscan Processing” feature.

QUANTIFICATION AND STATISTICAL ANALYSIS

Live imaging Videos (Videos S1–S6) were analyzed using the Imaris (Bitplane, Oxford Instruments, Concord MA) “spots” function over and track using retrograde motion with a max frame gap of 3. MS2 foci were assumed to be 1 μ m across with a z-axis point spread function estimation of 2 μ m. After tracking, both intensity sum and position csv files were exported and analyzed using a series of custom R scripts. Tracks are assigned a nuclear cycle and zone position by referencing a manually generated annotation file containing all frames where anaphase was reached for each Video and a y-axis position of ventral repression at nuclear cycle 14. Transcriptional delay values for each tracked object were generated by subtracting the current frame number by the preceding anaphase frame number. Transcriptional dynamics at different dorsal-ventral positions was analyzed by subdividing each image into five zones along the DV axis. Zone 1 comprises the mesoderm, as determined by the Snail repression border that becomes obvious in early NC14. The remaining zones are defined by 20 μ m spatial bins that proceed dorsally, approximately 4 rows of nuclei per zone (schematized in Figure 2C).

To measure transcriptional kinetic parameters, we used individual foci and performed a linear fit on the first 25% of the intensity values over time. Time to steady-state values were calculated by intersecting the linear fit with a horizontal line generated by the averaging the top 20% of intensity values for foci signals. Statistical tests were performed using Welch’s T-test that assumes independent underlying variance. P-values shown in Figure 3H are visually represented as one asterisk indicating a $p < 0.05$, two indicating $p < 0.01$, and three indicating $p < 0.001$.

The smFISH nascent transcript values shown in Figure 4 were obtained by extracting the total fluorescence of large nuclear localized foci assumed to be the point of active transcription. This value was then divided by intensity values of single transcripts by assuming an average 0.3 μ m diffraction limited point again using the Imaris “spots”. These values formed a normal distribution from which the median value was selected as the fluorescence intensity value of a single transcript within a single frame. DI intensity values for each nucleus were found by extracting the mean fluorescence of antibody stain signal within volumes defined by nuclear DAPI signal. This normalizes differences in DI concentrations along the gradient between genotypes. Radial scans were performed using a custom R script that utilized the position values extracted from Imaris to interrogate .tif files of the DI antibody stain. Error bars on enrichment plots in Figure 4C are standard error of the mean of individual enrichment curves in each positional bin. All plotting was performed with base R functions and the ggplot2 library.

DETAILED GENOTYPES:

Figure 1:

1A: $wt = \text{♀ } y[1] w[*] X \text{ ♂ } y[1] w[*]$

1B: zld^- prepared by zld RNAi in two crosses: 1st cross $\text{♀ } +; +; \text{UAS-shRNA-}zld X \text{ ♂ } P\{COG-GAL4:VP16\}; P\{Gal4-nos.NGT\}40; P\{nos-Gal4-VP16\}$; 2nd cross $G1 \text{♀ } P\{COG-GAL4:VP16\}/+; P\{Gal4-nos.NGT\}40/+; P\{nos-Gal4-VP16\}/\text{UAS-shRNA-}zld X \text{ ♂ } yw$

1D: 3TAG = $y[1] w[*]; sog\ 3TAG\text{-}MS2\text{-}lacZ;+$

1E: 0TAG = $y[1] w[*]; sog\ 0TAG\text{-}MS2\text{-}lacZ;+$

Figure 2:

2A, C, E: 3TAG ♀ $y[1] w[*]; P\{w[+mC]=His2Av\text{-}mRFP1\}II.2; P\{w[+mC]=nos\text{-}MCP.EGFP\}2\ X\ \sigma\ y[1] w[*]; sog\ 3TAG\text{-}MS2\text{-}lacZ;+$

2B, D, F: 0TAG ♀ $y[1] w[*]; P\{w[+mC]=His2Av\text{-}mRFP1\}II.2; P\{w[+mC]=nos\text{-}MCP.EGFP\}2\ X\ \sigma\ y[1] w[*]; sog\ 0TAG\text{-}MS2\text{-}lacZ;+$

Figure 3:

3B, D, F: 3TAG ♀ $y[1] w[*]; P\{w[+mC]=His2Av\text{-}mRFP1\}II.2; P\{w[+mC]=nos\text{-}MCP.EGFP\}2\ X\ \sigma\ y[1] w[*]; sog\ 3TAG\text{-}MS2\text{-}lacZ;+$

3C, E, F: 0TAG ♀ $y[1] w[*]; P\{w[+mC]=His2Av\text{-}mRFP1\}II.2; P\{w[+mC]=nos\text{-}MCP.EGFP\}2\ X\ \sigma\ y[1] w[*]; sog\ 0TAG\text{-}MS2\text{-}lacZ;+$

Figure 4:

4A, B, C: 3TAG $y[1] w[*]; sog\ 3TAG\text{-}MS2\text{-}lacZ;+$

4A, B, C: 0TAG $y[1] w[*]; sog\ 0TAG\text{-}MS2\text{-}lacZ;+$

Figure S1 (Related to Figure 4)

S1A, C, D: 3TAG $y[1] w[*]; sog\ 3TAG\text{-}MS2\text{-}lacZ;+$

S1B, C, D: 0TAG $y[1] w[*]; sog\ 0TAG\text{-}MS2\text{-}lacZ;+$

Videos (Related to Figures 2 and 3):

Video S1, S3, S5: **3TAG** $y[1] w[*]; sog\ 3TAG\text{-}MS2\text{-}lacZ;+$

Video S2, S4, S6: **0TAG** $y[1] w[*]; sog\ 0TAG\text{-}MS2\text{-}lacZ;+$

Supplementary Material

Refer to Web version on PubMed Central for supplementary material.

Acknowledgements

The authors would like to thank Shawn Little for the *lacZ* Atto633 smFISH probe, and Sirus Mrazik and Justin Kai-Ming Yeung for help with in situs. We also thank Edo Kussell, Carlos Carmona-Fontaine, Grace Aveçilla and Timothee Lionnet for helpful discussions regarding quantitative analysis of MS2 data, and Jonathan Liu, Jacques Bothma, and Stephen Small for insightful comments on the manuscript. The research was supported by a National Institute of Health research grant to CAR (GM63024). PHW was supported by a National Institute of Health training grant (5T32HD007520–20). HGG was supported by the Burroughs Wellcome Fund Career Award at the Scientific Interface, the Sloan Research Foundation, the Human Frontiers Science Program, the Searle Scholars Program, the Shurl & Kay Curci Foundation, the Hellman Foundation, the NIH Director's New Innovator Award (DP2 OD024541–01), and an NSF CAREER Award (1652236).

References:

1. Steward R, McNally FJ, and Schedl P (1984). Isolation of the dorsal locus of *Drosophila*. *Nature* 311, 262–265. [PubMed: 6434990]
2. Stathopoulos A, and Levine M (2002). Dorsal gradient networks in the *Drosophila* embryo. *Dev. Biol* 246, 57–67. [PubMed: 12027434]
3. Liang H-L, Nien C-Y, Liu H-Y, Metzstein MM, Kirov N, and Rushlow C (2008). The zinc-finger protein Zelda is a key activator of the early zygotic genome in *Drosophila*. *Nature* 456, 400–403. [PubMed: 18931655]
4. Schulz KN, Bondra ER, Moshe A, Villalta JE, Lieb JD, Kaplan T, McKay DJ, and Harrison MM (2015). Zelda is differentially required for chromatin accessibility, transcription factor binding, and gene expression in the early *Drosophila* embryo. *Genome Res* 25, 1715–1726. [PubMed: 26335634]
5. Nien C-Y, Liang H-L, Butcher S, Sun Y, Fu S, Gocha T, Kirov N, Manak JR, and Rushlow C (2011). Temporal coordination of gene networks by Zelda in the early *Drosophila* embryo. *PLoS Genet* 7, e1002339. [PubMed: 22028675]
6. Harrison MM, and Eisen MB (2015). Transcriptional Activation of the Zygotic Genome in *Drosophila*. *Curr. Top. Dev. Biol* 113, 85–112. [PubMed: 26358871]
7. Foo SM, Sun Y, Lim B, Ziukaite R, O'Brien K, Nien C-Y, Kirov N, Shvartsman SY, and Rushlow CA (2014). Zelda Potentiates Morphogen Activity by Increasing Chromatin Accessibility. *Curr. Biol* 24, 1341–1346. [PubMed: 24909324]
8. Sun Y, Nien C-Y, Chen K, Liu H-Y, Johnston J, Zeitlinger J, and Rushlow C (2015). Zelda overcomes the high intrinsic nucleosome barrier at enhancers during *Drosophila* zygotic genome activation. *Genome Res* 25, 1703–1714. [PubMed: 26335633]
9. Harrison MM, Li X-Y, Kaplan T, Botchan MR, and Eisen MB (2011). Zelda binding in the early *Drosophila melanogaster* embryo marks regions subsequently activated at the maternal-to-zygotic transition. *PLoS Genet* 7, e1002266. [PubMed: 22028662]
10. Mir M, Reimer A, Haines JE, Li XY, Stadler M, Garcia H, Eisen MB and Darzacq X, (2017). Dense Bicoid hubs accentuate binding along the morphogen gradient. *Genes Dev* 31, 1784–1794. [PubMed: 28982761]
11. Kanodia JS, Liang H-L, Kim Y, Lim B, Zhan M, Lu H, Rushlow CA, and Shvartsman SY (2012). Pattern formation by graded and uniform signals in the early *Drosophila* embryo. *Biophys. J* 102, 427–433. [PubMed: 22325264]
12. Larson DR, Zenklusen D, Wu B, Chao JA, and Singer RH (2011). Real-time observation of transcription initiation and elongation on an endogenous yeast gene. *Science* 332, 475–478. [PubMed: 21512033]
13. Forrest KM, and Gavis ER (2003). Live imaging of endogenous RNA reveals a diffusion and entrapment mechanism for nanos mRNA localization in *Drosophila*. *Curr. Biol* 13, 1159–1168. [PubMed: 12867026]
14. Garcia HG, Tikhonov M, Lin A, and Gregor T (2013). Quantitative imaging of transcription in living *Drosophila* embryos links polymerase activity to patterning. *Curr. Biol* 23, 2140–2145. [PubMed: 24139738]
15. Lucas T, Ferraro T, Roelens B, De Las Heras Chanes J, Walczak AM, Coppey M, and Dostatni N (2013). Live Imaging of Bicoid-Dependent Transcription in *Drosophila* Embryos. *Curr. Biol* 23, 2135–2139. [PubMed: 24139736]
16. Lucas T, Tran H, Romero CAP, Guillou A, Fradin C, Coppey M, Walczak AM, and Dostatni N (2018). 3 minutes to precisely measure morphogen concentration. (2018). 3 minutes to precisely measure morphogen concentration. *PLoS Genet* 14, e1007676 [PubMed: 30365533]
17. Wu B, Miskolci V, Sato H, Tutucci E, Kenworthy CA, Donnelly SK, Yoon YJ, Cox D, Singer RH, and Hodgson L (2015). Synonymous modification results in high-fidelity gene expression of repetitive protein and nucleotide sequences. *Genes Dev* 29, 876–886. [PubMed: 25877922]
18. Hong J-W, Hendrix DA, and Levine MS (2008). Shadow enhancers as a source of evolutionary novelty. *Science* 321, 1314. [PubMed: 18772429]

19. Ozdemir A, Ma L, White KP, and Stathopoulos A (2014). Su(H)-mediated repression positions gene boundaries along the dorsal-ventral axis of *Drosophila* embryos. *Dev. Cell* 31, 100–113. [PubMed: 25313963]
20. Saint R, and Clarkson M (2000). Pictures in cell biology. A functional marker for *Drosophila* chromosomes in vivo. *Trends Cell Biol* 10, 553. [PubMed: 11121748]
21. Kanodia JS, Rikhy R, Kim Y, Lund VK, DeLotto R, Lippincott-Schwartz J, and Shvartsman SY (2009). Dynamics of the Dorsal morphogen gradient. *Proc. Natl. Acad. Sci. U. S. A* 106, 21707–21712. [PubMed: 19996178]
22. Liberman LM, Reeves GT, and Stathopoulos A (2009). Quantitative imaging of the Dorsal nuclear gradient reveals limitations to threshold-dependent patterning in *Drosophila*. *Proc. Natl. Acad. Sci. U. S. A* 106, 22317–22322. [PubMed: 20018754]
23. Reeves GT, Trisnadi N, Truong TV, Nahmad M, Katz S, and Stathopoulos A (2012). Dorsal-ventral gene expression in the *Drosophila* embryo reflects the dynamics and precision of the dorsal nuclear gradient. *Dev. Cell* 22, 544–557. [PubMed: 22342544]
24. Mir M, Stadler MR, Ortiz SA, Hannon CE, Harrison MM, Darzacq X, and Eisen MB (2018). Dynamic multifactor hubs interact transiently with sites of active transcription in embryos. *Elife* 7 Available at: 10.7554/eLife.40497.
25. Dufourt J, Trullo A, Hunter J, Fernandez C, Lazaro J, Dejean M, Morales L, Nait-Amer S, Schulz KN, Harrison MM, et al. (2018). Temporal control of gene expression by the pioneer factor Zelda through transient interactions in hubs. *Nat. Commun* 9, 5194. [PubMed: 30518940]
26. He F, Ren J, Wang W, and Ma J (2011). A Multiscale Investigation of Bicoid-Dependent Transcriptional Events in *Drosophila* Embryos. *PLoS One* 6, e19122. [PubMed: 21544208]
27. Xu H, Sepúlveda LA, Figard L, Sokac AM, and Golding I (2015). Combining protein and mRNA quantification to decipher transcriptional regulation. *Nat. Methods* 12, 739–742. [PubMed: 26098021]
28. Little SC, Tikhonov M, and Gregor T (2013). Precise Developmental Gene Expression Arises from Globally Stochastic Transcriptional Activity. *Cell* 154, 789–800. [PubMed: 23953111]
29. Tsai A, Muthusamy AK, Alves MR, Lavis LD, Singer RH, Stern DL, and Crocker J (2017). Nuclear microenvironments modulate transcription from low-affinity enhancers. *Elife* 6 Available at: 10.7554/eLife.28975.
30. Li X-Y, and Eisen MB (2018). Zelda potentiates transcription factor binding to zygotic enhancers by increasing local chromatin accessibility during early *Drosophila melanogaster* embryogenesis Available at: 10.1101/380857.
31. Xu Z, Chen H, Ling J, Yu D, Struffi P, and Small S (2014). Impacts of the ubiquitous factor Zelda on Bicoid-dependent DNA binding and transcription in *Drosophila*. *Genes Dev* 28, 608–621. [PubMed: 24637116]
32. Groth AC, Fish M, Nusse R, and Calos MP (2004). Construction of transgenic *Drosophila* by using the site-specific integrase from phage phiC31. *Genetics* 166, 1775–1782. [PubMed: 15126397]
33. Bischof J, Maeda RK, Hediger M, Karch F, and Basler K (2007). An optimized transgenesis system for *Drosophila* using germ-line-specific phiC31 integrases. *Proc. Natl. Acad. Sci. U. S. A* 104, 3312–3317. [PubMed: 17360644]
34. Hertz GZ, and Stormo GD (1999). Identifying DNA and protein patterns with statistically significant alignments of multiple sequences. *Bioinformatics* 15, 563–577. [PubMed: 10487864]
35. Francois V, Solloway M, O'Neill JW, Emery J, and Bier E (1994). Dorsal-ventral patterning of the *Drosophila* embryo depends on a putative negative growth factor encoded by the short gastrulation gene. *Genes Dev* 8, 2602–2616. [PubMed: 7958919]

Highlights

The expression domain of the Dorsal target-gene *sog* narrows in the absence of Zelda
Using MS2 reporter transgenes, this can be accurately recapitulated in living embryos
Without Zelda, the onset and degree of reporter activation becomes graded like Dorsal
Zelda promotes accumulation of Dorsal protein at the site of the enhancer

Author Manuscript

Author Manuscript

Author Manuscript

Author Manuscript

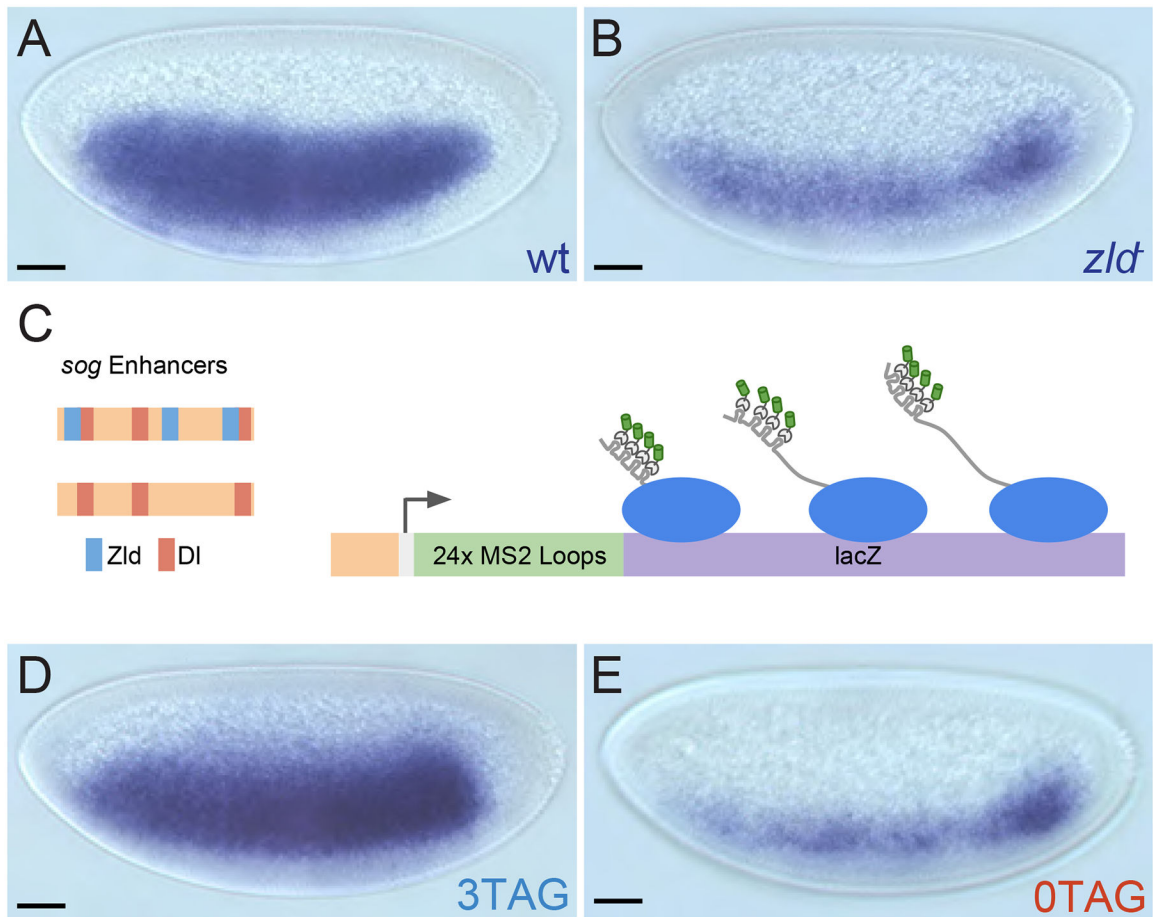


Figure 1: Zld potentiates DI activity at the *sog* enhancer.

(A-B) Conventional enzymatic *in situ* hybridization staining of *sog* in wild type and *zld* mutant NC14 embryos. (C) Schematic representation of transgenes. MS2 loops have been incorporated into the 5' end of the transcript upstream of a *lacZ* reporter sequence. (D-E) *in situ* hybridization staining of the engineered MS2v5(-TAG) *lacZ* transgenic embryos, showing that 3TAG and 0TAG expression is similar to the expression of *sog* in wild type and *zld* mutants, respectively.

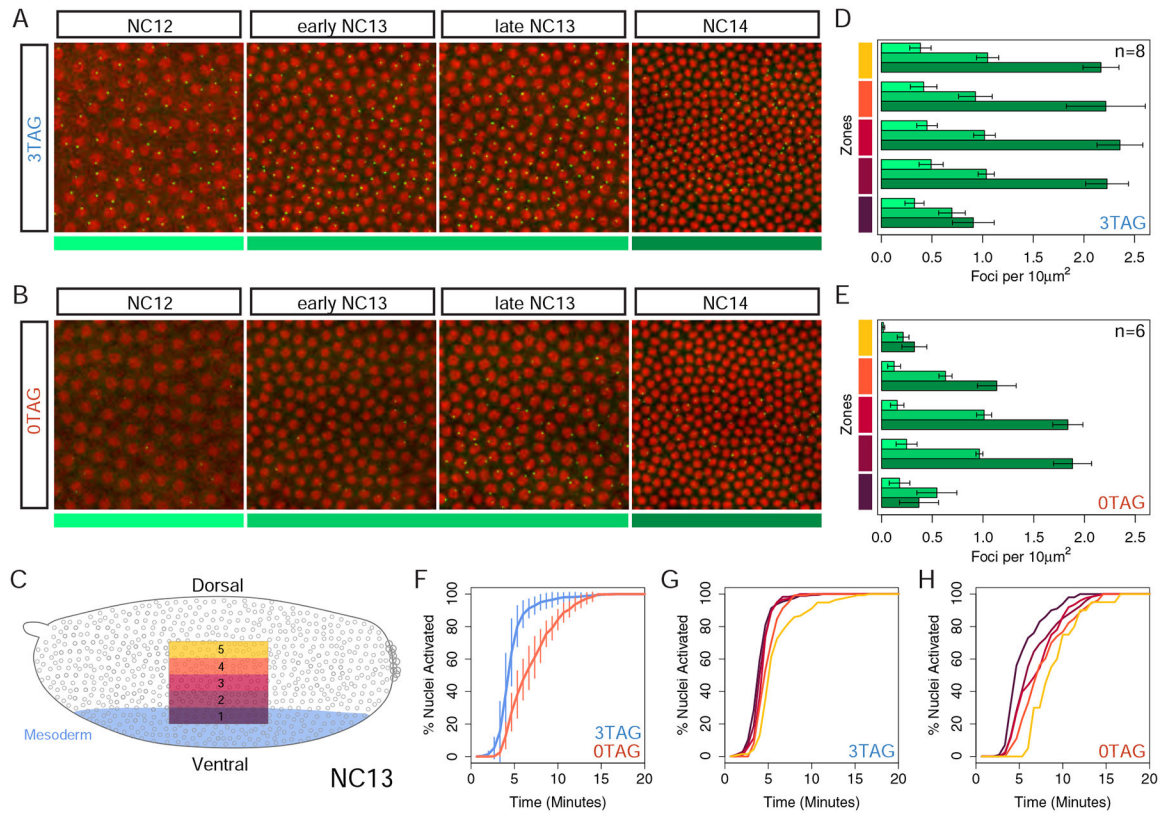


Figure 2: MS2 imaging reveals a position dependent transcriptional delay in the absence of Zld binding sites.

(A-B) Frames taken from live imaging Videos S1 and S2 that track transcription (green spots) from NC12 to NC14 as indicated and color coded below, NC12 (light green), NC13 (medium green), NC14 (dark green). Nuclei (red) have been labeled using maternally loaded H2Av-RFP. Bars on right side follow five zones along the dorsal/ventral axis with ventral mesoderm on bottom (Zone 1) as diagrammed in the embryo schematic (C) with blue shading defining the presumptive mesoderm of the embryo. (D-E) Quantification of the number of expressing nuclei in NC12 to NC14 (color coded as in A-B) agrees with conventional in situ analysis, showing markedly fewer active nuclei in 0TAG embryos across consecutive nuclear cycles, especially in Zones 4 and 5. In total, 8 3TAG embryos and 6 0TAG embryos were analyzed as indicated in the bar plots, and plotted with error bars representing one standard deviation of all values collected for each cycle and bin. For additional videos, see Videos S3–S6. (F-H) Cumulative distribution curves of nuclei that activate transcription in NC13, excluding nuclei that never activate in NC13. Time 0 on the X-axis is the start of anaphase of the previous cycle, NC12. All zones concatenated with delay values across genotypes in (F) with variance across biological replicates indicated with vertical lines showing one standard deviation of all embryos measured. 3TAG embryos activate transcription simultaneously across the expression domain (G), and 0TAG embryos show a delay dependent on the nucleus' position in the DI gradient (H).

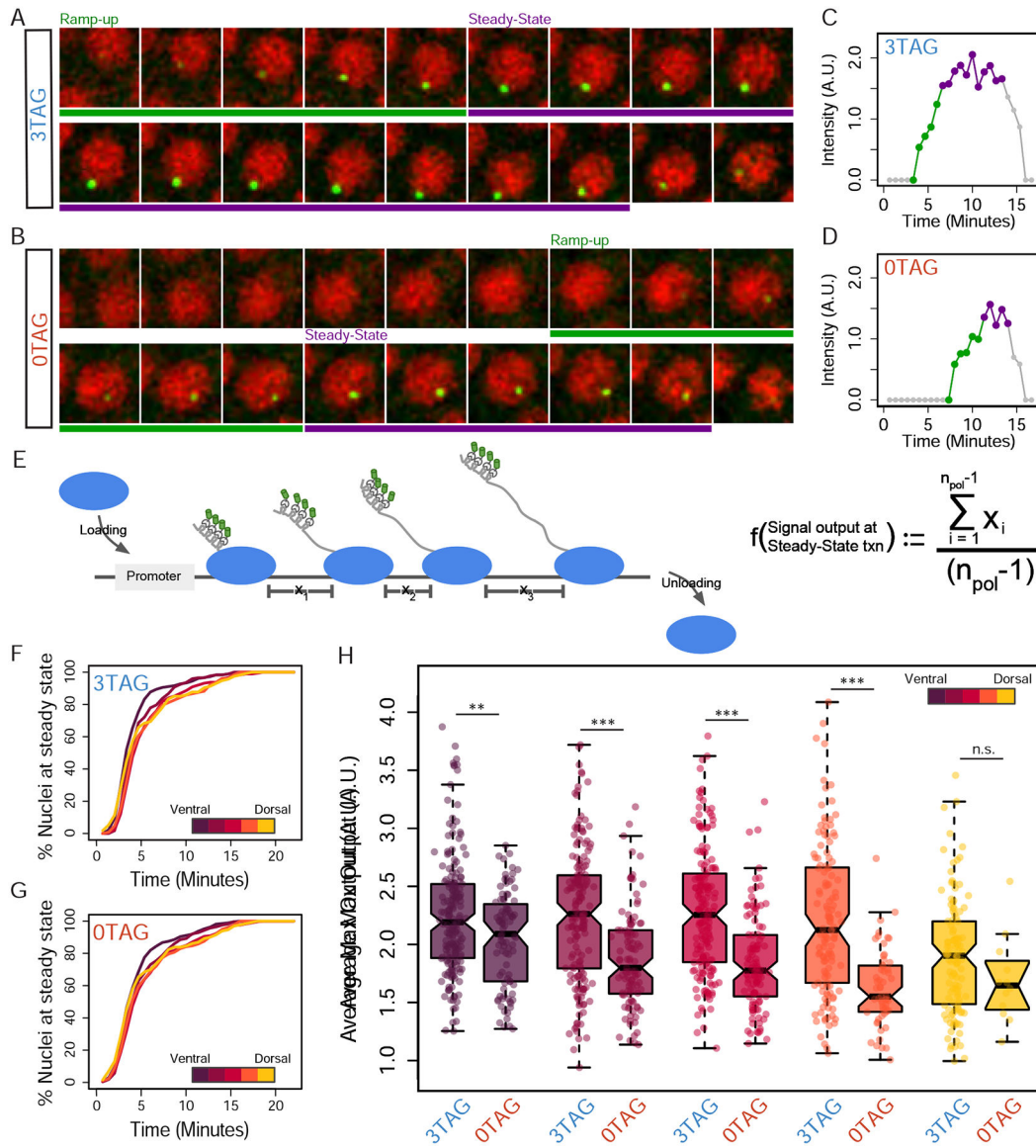


Figure 3. Zld promotes full saturation of polymerase on the gene body during transcriptional elongation.

(A-B) Representative single nuclei tracked over NC13 from Videos S1 (A) and S2 (B). Time stamp (min) shown in bottom right corner of each frame (Time 0 is defined as the start of NC12 anaphase). Ramp-up and Steady-state phases of transcription are highlighted with green and purple bars, respectively. (C-D) Quantification of signal intensity over time from representative nuclei shown. Phases of transcription are highlighted with corresponding colors as in A and B. Ramp-up is calculated as the length of time between detection above background of the MS2 focus and max output (averaged; see STAR Methods). (E) Schematic representation of steady-state transcription, where the gene body is decorated with elongating RNA polymerases, and the rate of loading is roughly matched by the rate of unloading. X values show the spacing between polymerase molecules. Spacing of polymerase molecules can be inferred from the signal output at steady-state using the equation shown. (F-G) Cumulative distribution curves of the percentage of nuclei that have

reached steady-state. (H) Average intensity at steady-state (NC13) plotted as box plot distributions over all five zones of the *sog* expression domain. In total for all zones, 855 and 460 nuclei were analyzed for 3TAG and 0TAG, respectively, from 8 3TAG and 6 0TAG embryos (see additional Videos S1–S6). Significant differences between all zones except Zone 5 were found using a Welch's t-test between the genotypes. 3TAG embryos show little difference over the first four zones, while 0TAG embryos show progressive loss in signal intensity over the dorsal/ventral axis.

Author Manuscript

Author Manuscript

Author Manuscript

Author Manuscript

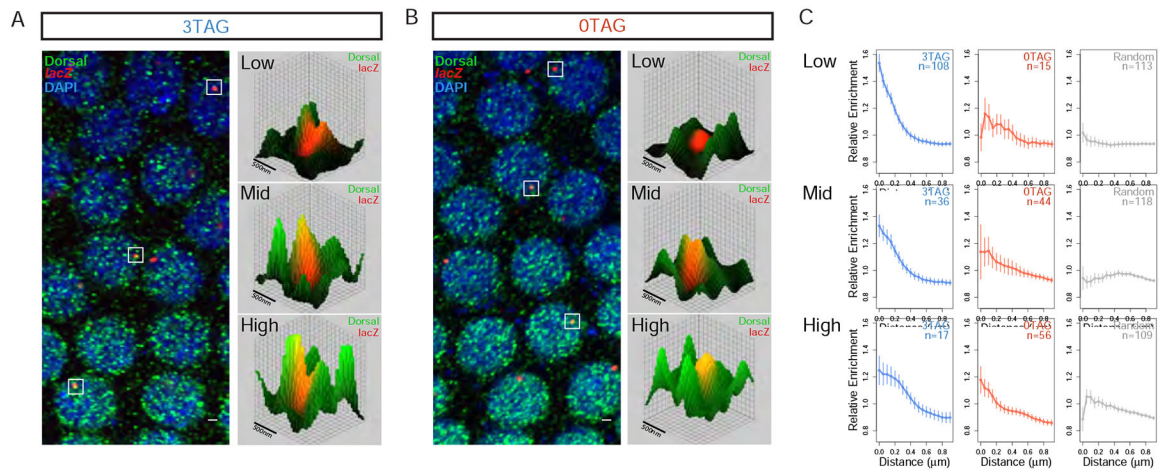


Figure 4. Zld increases the local concentration of DI at the site of transcription.

(A-B) Confocal images of NC13 embryos stained with anti-DI antibodies and smFISH probes for the *lacZ* reporter genes 3TAG (A) and OTAG (B). DI staining appears highly punctate, indicating the possible presence of high-DI nuclear microenvironments. Sites of active transcription are visualized as red nuclear foci that can be localized in 3D space. Select foci were isolated and visualized in 3D contour maps, where the height of surface represents the intensity of the DI staining. A high incidence of FISH signal overlapping with DI microdomains was observed, suggesting the concentration of DI may have an impact on transcription. (C) The distributions of DI signal within the microdomain of transcribing foci (see Figure S1 for individual enrichment curves). In regions of high nuclear DI, both genotypes show similar distributions, but a difference is detected in regions where nuclear DI begins to drop. Control distributions were prepared using random places in the nucleus. The numbers of nuclei (n) used for the analysis are indicated. Three embryos for each genotype were used. Error bars: standard error of the mean.

KEY RESOURCES TABLE

REAGENT or RESOURCE	SOURCE	IDENTIFIER
Antibodies		
Sheep anti-DIG-AP antibody	Roche	Cat# 11093274910, RRID:AB_2734716
Mouse anti-DL antibody (7A4)	Developmental Studies Hybridoma Bank	Cat# anti-Dorsal 7A4, RRID:AB_528204
Alexa fluor 488 goat anti mouse secondary antibody	ThermoFisher Scientific	Cat# A-11001, RRID:AB_2534069
Chemicals, Peptides, and Recombinant Proteins		
5-Bromo-4-chloro-3-indolyl phosphate p-toluidine salt(BCIP)	Roche	Cat# 10760994001
4-Nitro blue tetrazolium chloride(NBT)	Roche	Cat# 11585029001
DIG RNA labeling mix	Roche	Cat# 11277073910
RNA FISH Hybridization Buffer	Stellaris (LGC Biosearch Technologies)	Cat# SMF-HB1-10
DAPI	Sigma-Aldrich	Cat# D9542
Aqua-Poly/Mount	Polysciences	Cat# 18606-20
Number 1.5 glass coverslips	Fisher Scientific	Cat# 22266858
Gibson Assembly Master Mix	New England Biolabs, Inc	Cat# E2611S
<i>lacZ</i> Atto633 smFISH Probe	Shawn Little's lab	[28]
<i>lacZ</i> ISH DIG RNA Probe	This lab	
<i>sog</i> ISH DIG RNA Probe	This lab	
Experimental Models: Drosophila Strains		
<i>y[1] w[1118]</i>	Bloomington Drosophila Stock Center	Cat# 6598
<i>y[1] w[*]; P{ w[+mC]=His2Av-mRFP1 }II.2; P{ w[+mC]=nos-MCP.EGFP }2</i>	Bloomington Drosophila Stock Center	Cat# 60340, RRID:BDSC_60340
Maternal Triple Driver(MTD)-Gal4: P{ <i>COG-GAL4:VP16</i> }; P{ Gal4- <i>nos</i> .NGT }40; P{ <i>nos</i> -Gal4-VP16 }	Bloomington Drosophila Stock Center	Cat# 31777, RRID:BDSC_31777
UAS-shRNA- <i>zld</i>	This lab	[8]
<i>sog</i> 3TAG-MS2- <i>lacZ</i>	This paper	N/A
<i>sog</i> 0TAG-MS2- <i>lacZ</i>	This paper	N/A
Recombinant DNA		
<i>pib</i> -evepr-ms2v5(-TAG)- <i>lacZ</i> plasmid	This paper	N/A
Software and Algorithms		
FIJI (ImageJ)	NIH	http://fiji.sc
Matlab	The Mathworks Inc.	https://www.mathworks.com
Imaris	Bitplane	www.bitplane.org
R	The R Foundation	https://www.r-project.org
LAS X	Leica Microsystems Inc	https://www.cellularimaging.nl/leica-las-x/
N2012	CarlZE Zeiss Inc	https://www.zeiss.com/corporate/int/home.html
Other		

REAGENT or RESOURCE	SOURCE	IDENTIFIER
Confocal microscope	Leica	SP8
Confocal microscope	Zeiss	LSM 880
Microscope	Zeiss	Axioskop
Digital camera for microscopy	Zeiss	AxioCam MRc
Power meter(X-cite)	Lumen Dynamics Group Inc, Canada	Model # XR2100
Breathable membrane (Lumox Film)	Sarstedt AG & Co.; Nümbrecht, Germany	Cat# 94.6077.317
Plastic microscope slide (3D printed)	Sculpteo; Créteil, France	N/A

Author Manuscript

Author Manuscript

Author Manuscript

Author Manuscript